J Mater Sci (2007) 42:8279–8286
DOI 10.1007/s10853-007-1644-4

# The electrochemical behaviour of nitrogen-containing austenitic stainless steel in methanolic solution

**V. B. Singh · Monali Ray**

Received: 28 June 2006 / Accepted: 27 February 2007 / Published online: 19 June 2007


**Abstract** The corrosion behaviour of nitrogen-containing austenitic stainless steel in methanol containing different concentrations of $H_2SO_4$, HCl, LiCl and $H_2SO_4$ + HCl has been investigated using a potentiostatic polarization method. The cathodic reaction in the $H_2SO_4$, HCl and $H_2SO_4$ + HCl solutions was proton reduction whereas in the neutral LiCl solution, oxygen reduction was the predominant cathodic reaction. Active, passive and transpassive behaviours were observed only for higher concentrations of $H_2SO_4$ (0.01–2.0 M) due to the inherent water content. A cathodic loop, characterized by measured negative current in the anodic region, was also observed in solutions, in which the concentration of $H_2SO_4$ was 1.0 M or higher. The relative stability of the passive films decreased as the $H_2SO_4$ concentration increased, and thus the steel suffered from mild pitting corrosion. In the chloride environment, the rate of corrosion increased as the $Cl^-$ ion concentration increased. The presence of acid along with $Cl^-$ ions enhanced corrosion, and the corrosion rate increased significantly. The steel suffered from mild intergranular corrosion in acidic chloride solutions of methanol. In the $H_2SO_4$ + HCl solutions, passive films were only formed when the $H_2SO_4$ to HCl concentration ratio was greater than ~10:1.

## Introduction

Austenitic stainless steels are extensively used as structural materials for a wide variety of chemical and industrial applications due to their high mechanical strength, ductility and excellent corrosion resistance. The composition of these steels can be tailored in order to obtain improved properties and corrosion resistance. Nitrogen is a very effective alloying addition to obtain an increase in strength as well as corrosion resistance. It offers excellent resistance against pitting corrosion due to the formation of protective nitrogen-rich oxide deposits [1, 2], and prevents the attack of anions ($Cl^-$). Even in an acidic environment, the segregated nitrogen ($N^{3-}$) reacts with $H^+$ ions in the solution leading to a higher pH, and thus retards the extent of corrosion. Pitting is also hindered by the formation of $NO_3^-$ ions in aqueous solution [3]. Moreover, nitrogen is a very good austenitic stabilizer [4, 5], so that lower nickel contents can be used and still retain the single austenitic phase. Reducing the nickel content in stainless steel results in lower costs of production. Therefore, the new nitrogen-containing austenitic stainless steels are regarded as one of the frontier areas of research in the field of metallic materials.

The corrosion behaviour of nitrogen-containing steels in neutral and acidic aqueous solutions has been investigated previously [1, 2, 6–9]. However, very little information concerning the corrosion behaviour of these steels in non-aqueous solvents is available in literature. Among non-aqueous solvents, methanol is the one most widely used in fuel cells (direct methanol fuel cell) as a source of hydrogen and as an alternative fuel for oil in automobiles. There is growing concern about the corrosion of stainless steels in methanol, especially in the presence of acids and aggressive halide ions [10], because an acid has deleterious effect on metal dissolution due to promotion of the cathodic reaction (proton reduction), and $Cl^-$ and $Br^-$ ions have stimulating effects even at very low concentrations on the dissolution of the metal.

V. B. Singh (✉) · M. Ray
Department of Chemistry, Banaras Hindu University,
Varanasi 221 005, India
e-mail: vijaybs@bhu.ac.in

The aim of this paper is to study the effects of acid and chloride ions on the electrochemical behaviour of nitrogen-containing austenitic stainless steel in methanolic solution.

## Experimental procedure

The chemical composition (wt.%) of the working electrode material (steel) is Cr, 14.0%; Mn, 8.75%; Ni, 0.8%; Cu, 1.48%; Si, 0.5%; C, 0.11%; N, 0.14% and balance Fe (M/S Mehta Alloys Limited, Ahmedabad). The working electrode (steel) was polished mechanically to a mirror finish using successive grades of emery paper followed by polishing with alumina powder. It was then washed thoroughly with bidistilled water, degreased with acetone and transferred quickly into the electrochemical cell.

The cell used was a conventional three-electrode all-glass electrochemical cell consisting of a working electrode, a platinum counter electrode of large surface area and a saturated calomel reference electrode (SCE). Details of experimental setup and working procedures are described elsewhere [11, 12].

The electrochemical polarization experiments were carried out using a potentiostat (Wenking POS 73). The working electrode specimen of 2 $cm^2$ exposed area was immersed in the experimental solution for 30 min to stabilize the open-circuit potential (OCP). The polarization was performed potentiostatically by starting at a negative potential and then moving towards positive potential. The potential was stepped in 20 mV/min. All measured potentials were referred to saturated calomel electrode (SCE). All measurements were performed in aerated solution at 35 ± 1 °C without any stirring. Stock solutions of 2.0 M $H_2SO_4$, 1.0 M HCl and 0.5 M LiCl, respectively, were prepared using analytical grades of chemicals in distilled purified methanol.

After the experiment was completed, the specimens were rinsed in deionized water in an ultrasonic bath and were subsequently examined using a scanning electron microscope (Philips XL-20). For the determination of metal ions in solution (after electrochemical studies), spectral analysis was performed using a CARY 2390 spectrophotometer.

## Results and discussion

### Methanol–$H_2SO_4$

The OCP of the alloy in methanol containing different concentrations of $H_2SO_4$ (0.001–2.0 M) ranged between –150 and –57 mV. The cathodic and anodic polarization curves of the steel are illustrated in Fig. 1(a). The cathodic

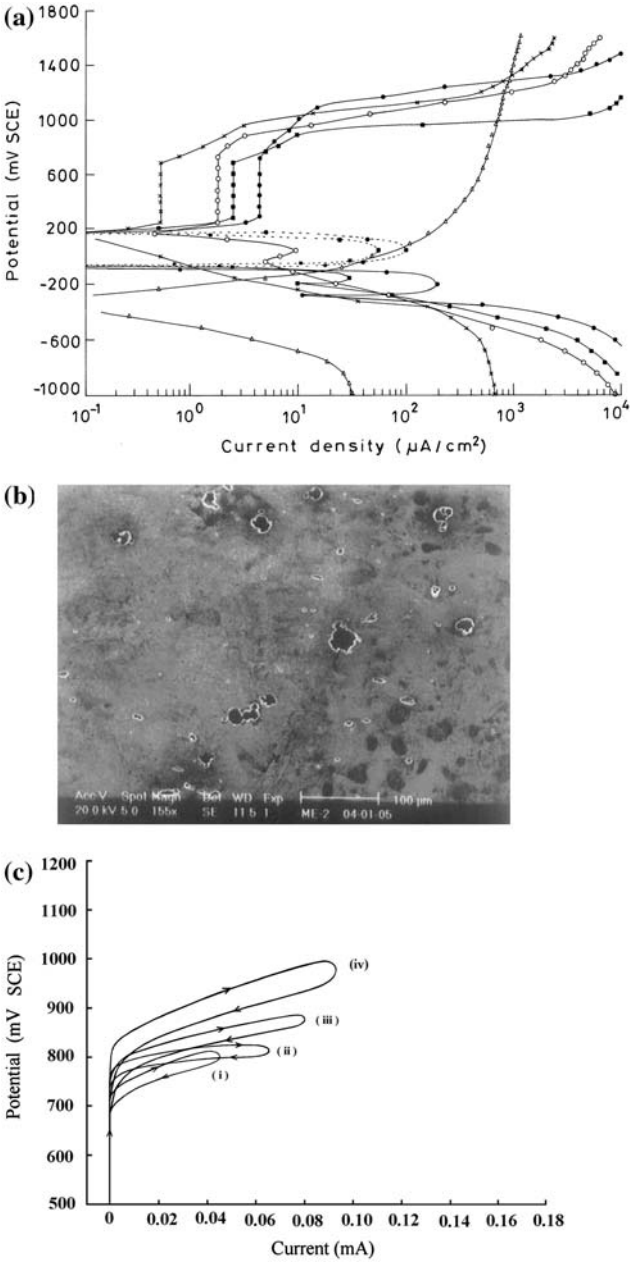


**Fig. 1** (**a**) Polarization curves of nitrogen-containing austenitic stainless steel in different concentrations of $H_2SO_4$ in methanol, at 35 °C. (i) △—△0.001 M $H_2SO_4$, (ii) ×—× 0.01 M $H_2SO_4$, (iii)○—○ 0.1 M $H_2SO_4$, (iv) ■—■ 1.0 M $H_2SO_4$ and (v) 2.0 M $H_2SO_4$. (**b**) SEM micrograph of nitrogen-containing austenitic stainless steel after polarization in 0.1 M $H_2SO_4$ in methanol. (**c**) Cyclic anodic polarization curve of nitrogen-containing austenitic stainless steel in different concentrations of $H_2SO_4$ in methanol, at 35°C. (i) 0.01 M $H_2SO_4$, (ii) 0.1 M $H_2SO_4$, (iii) 1.0 M $H_2SO_4$ and (iv) 2.0 M $H_2SO_4$

Tafel slopes ($b_c$) in most cases ranged from 120 to 160 mV/dec, which indicated that the cathodic process is the activation controlled hydrogen evolution reaction. In 0.001 and 0.01 M $H_2SO_4$–methanol, the limiting current was observed at higher negative potentials (–800 mV for

0.001 M and –600 mV for 0.01 M $H_2SO_4$). Similar results have been reported for 9Cr–1Mo steel in $H_2SO_4$–methanol solutions [13]. Therefore, the limiting currents were due to the very low concentrations of $H^+$ ions in the solution.

The anodic polarization curves for the steel in 0.01 to 2.0 M $H_2SO_4$–methanol solutions can be clearly divided into three potential regions: the active region associated with a large anodic current peak followed by the passive region with a constant and lower current density, and the transpassive region, where the current again increases rapidly. However, an active–passive transition was not observed in the 0.01 M $H_2SO_4$ solution. In the active region, the critical current density for passivation ($i_{crit}$) increased as the concentration of $H_2SO_4$ in methanol increased in the order 0.1 M < 1.0 M < 2.0 M (Table 1). The corrosion current density ($i_{corr}$) also increased as the concentration of $H_2SO_4$ increased from 0.01 to 2.0 M. The increase in $i_{crit}$ and $i_{corr}$ were likely due to the increase in acidity of the solution. In this region, iron presumably dissolved with a higher current density than in the passive region. The prepassive region followed; in this region, the overall anodic reaction was likely to be:

$$(Fe, Cr) + H_2SO_4 = (Fe, Cr)SO_4 + H_2 \quad (1)$$

The prepassive layers appeared to consist mainly of $Cr(OH)_3$, $Cr_2(SO_4)_3$ and a minor cationic fraction of Fe(II) [14], which differed from the passive films in composition.

A remarkable feature was noticed for 1.0 and 2.0 M $H_2SO_4$ solutions: negative currents were observed between potentials –100 and 160 mV. The negative current observed in the anodic polarization region is described as a 'cathodic loop', which is shown in Fig. 1a (dashed lines). Such a 'cathodic loop' had been observed earlier in different solutions [15–19]. Greene [17] and Lee et al. [18] have interpreted existence of the loop as due to oxygen reduction even in the helium-saturated solution. Frankenthal [19] suggested that hydrogen evolution was the cause for the loop. Therefore, in the present case, oxygen reduction may be the reason for the presence of such a cathodic loop. However, the role of copper in this potential region cannot be ruled out, since the stainless steel contains 1.48 wt.% copper. The surface of the steel undergoes a selective dissolution of the more active constituents, leading to the accumulation of copper on the surface, on which the reduction of hydrogen takes place due to the lower hydrogen overvoltage [20].

Stable passive films formed in all the methanol–$H_2SO_4$ solutions except 0.001 M solution. The passivation potentials ($E_{pass}$) and breakdown potentials ($E_{break}$) were roughly the same irrespective of $H_2SO_4$ concentration (Fig. 1a). The stability of the passive films may be due to the existing water in $H_2SO_4$. Water plays a significant role in the formation and stability of passive films [21–23]. For the formation of a stable passive film, a certain minimum concentration of water is required, known as the ''critical water concentration'', which depends on the material. In the present case, the water contents of the respective solutions were higher than the critical concentration to render stable passive film formation. XPS investigations on the passive film formed on Fe–Cr–Mn alloys have shown that it is a mixture of iron, chromium and manganese oxides ($Cr_2O_3$, $Fe_2O_3$, $Mn_2O_3$, etc.) [19, 24, 25]; chromium probably being a hydrated chromium oxyhydroxide [26]. In fact, it is a bilayer structure consisting of inner oxide layer and outer hydroxide layer. When stainless steel is exposed to acidic environments, a chromium rich oxide-hydroxide film is formed on the surface, which proceeds by solid-state mechanisms as:

$$4Cr + 3H_2SO_4 = 2Cr_2O_3 + 3SO_2 + 6H^+ + e^- \quad (2)$$

$$Cr + H_2SO_4 = CrOOH + SO_2 + H^+ + e^- \quad (3)$$

The chromium enrichment is due to the preferential dissolution of iron and manganese into the solution and low mobility of chromium in the film. In case of the nitrogen-containing steel, the passive film also contains nitrogen in it in the form of CrN [4, 27].

In the present investigation, the passive potential range was found to be almost the same irrespective of the concentration of $H_2SO_4$ in the solution; but the passivation current density ($i_p$) increased in the order

**Table 1** Corrosion parameters of nitrogen-containing austenitic stainless steel in different concentrations of $H_2SO_4$ in methanol, at 35 °C

| Conc. of $H_2SO_4$ (M) | $E_{corr}$ (mV) | $i_{corr.}$ (μA/cm$^2$) | $i_{crit.}$ (μA/cm$^2$) | $i_p$ (μA/cm$^2$) | $E_{pass}$ (mV) | $E_{break}$ (mV) | $E_{pit}$ (mV) | $\Delta E$ ($E_{pit}$ ~ $E_{break}$) (mV) |
|---|---|---|---|---|---|---|---|---|
| 0.001 | –340 | <0.1 | – | – | – | – | – | – |
| 0.01 | 150 | 0.11 | – | 0.52 | 240 | 680 | 960 | 280 |
| 0.1 | –60 | 4.9 | 9.6 | 1.8 | 240 | 720 | 880 | 160 |
| 1.0 | –200 | 12 | 30 | 2.5 | 280 | 680 | 880 | 200 |
| 2.0 | –340 | 13 | 200 | 4.4 | 280 | 720 | 1080 | 360 |

0.01 M < 0.1 M < 1.0 M < 2.0 M $H_2SO_4$, which showed that the passive films tend to be relatively more unstable with higher $i_p$ as the solution was becoming more and more acidic. This trend of $i_p$ variation was contrary to the findings of Mansfeld [28], where $i_p$ was reported to decrease with increase in $H_2SO_4$ concentration. The observed difference in the effect of $H_2SO_4$ on the passive current behaviour may be ascribed to a different alloy composition. The breakdown potential ($E_{break}$) was almost the same (~700 mV) in all the cases. The breakdown of the passive film can be associated with: (a) the dissolution Cr(III) compounds as soluble $Cr_2O_7^{2-}$ ions; (b) evolution of a gas, probably oxygen; and (c) localized attack on the passive film in the form of pitting. Scanning electron microscopy (SEM) showed the presence of shallow and small pits with a width of ~ 40 μm on the alloy surface (Fig. 1b). Therefore, the film breakdown here was due to pitting corrosion. This is also evident from the cyclic anodic polarization curve (Fig. 1c). Though pitting seemed to occur here, the extent of the attack was very weak. This may be probably due to the beneficial effect of nitrogen in the steel, which offers very good resistance against pitting. During the dissolution and the passivation process, nitrogen was expected to be enriched at the surface by segregation and weakened the attack of pitting.

It is noted that at the end of the passive region (i.e., between passive and transpassive potentials), where the anodic polarization curves could be characterized by two well-defined breaks at two specific potentials. The first break could be assigned as the breakdown potential ($E_{break}$) and the second one as the pitting potential ($E_{pit}$). The region between the two potentials (i.e., $\Delta E = E_{pit} - E_{break}$) was linear. Therefore, it could be suggested that at $E_{break}$, the breakdown of the passive film occured leading to the pit initiation. Along $\Delta E$, as the potential is increased, propagation of pits occured, but slowly (as indicated by gradual increase in the current in this region), and at $E_{pit}$, the growing pits became stable. The $\Delta E$ was found to increase as the concentration of $H_2SO_4$ (except 0.01 M) increased, which indicated that the stable pit formation was delayed as the concentration of $H_2SO_4$ was increased from 0.1 to 2.0 M. Similar results have been reported by El-Naggar [29] for carbon steel in 0.5 M $NaHCO_3$ containing chloride ions. According to him, at $E_{break}$, the adsorption of chloride ions occurred on the passive film followed by penetration and chemical interaction leading to the initiation of pitting, and at $E_{pit,}$ stable pits were formed due to the interaction of chloride ions with the bare metal surface. As reported previously [30], the pitting event occurred in the present case too, though the solution was free from chloride ions.

In the transpassive region at potential >1400 mV, limiting currents were observed due to the mass-transport controlled reaction and it increased as the concentration of $H_2SO_4$ in methanol increased. In this region, a gas evolved (most probably the oxygen), which commenced exactly at the initiation potential leading to a limiting current.

In 0.001 M $H_2SO_4$–methanol, only active anodic dissolution was observed. From the corrosion potential ($E_{corr}$), the current increased steeply followed by limiting nature at a potential >~600 mV which was probably due to the nucleation and growth of a salt film on the electrode–electrolyte interface. Such limiting currents have been observed earlier for copper in strong $H_2SO_4$ solutions [31]. No passive film was formed in this case because the concentration of $H_2SO_4$ (0.001 M) was too low to induce any passivity.

## Methanol–HCl

The OCP of the alloy in methanol containing different concentrations of HCl (0.001–1.0 M) ranged between –180 and –120 mV. The cathodic and anodic polarization curves in methanol–HCl solutions are depicted in Fig. 2a. The cathodic reaction occurring was the reduction of hydrogen ions and the cathodic current density increased as the concentration of HCl increased. The anodic curves indicated the active dissolution only where the aggressive chloride ions ($Cl^-$) prevented the passivation to occur. The

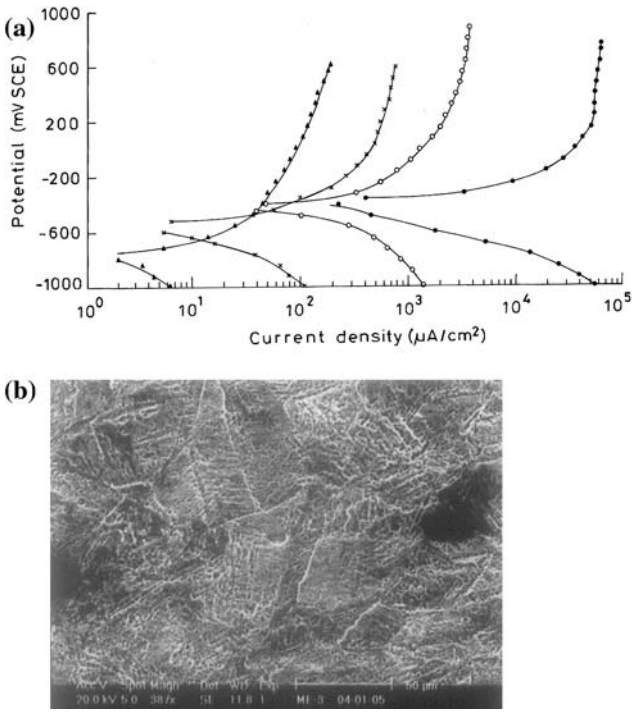


**Fig. 2** (**a**) Polarization curves of nitrogen-containing austenitic stainless steel in different concentrations of HCl in methanol, at 35 °C. (i)▲—▲ 0.001 M HCl, (ii)×—× 0.01 M HCl, (iii)o—o 0.1 M HCl and (iv) •—• 1.0 M HCl. (**b**) SEM micrograph of nitrogen-containing austenitic stainless steel after polarization in 0.1 M HCl in methanol

anodic Tafel slopes ($b_a$) in all the concentrations ranged between 60 and 90 mV/dec. The corrosion current ($i_{corr}$) increased in the order 0.001 < 0.01 < 0.1 < 1.0 M. The $i_{corr}$ for 0.001 M concentration of HCl was 1.1 μA/cm$^2$ whereas it became 190 μA/cm$^2$ in 1.0 M HCl. An increase in the concentration of HCl increased the chloride ion concentration and the acidity of the solution. The synergistic effects of the $Cl^-$ ions and the acid thus enhanced the rate of corrosion in higher HCl concentrations. General activating effect of $Cl^-$ ions on metal dissolution has been reported [32, 33] earlier also.

The nature of the curves was almost similar, where the current initially increased largely from $E_{corr}$ and thereafter at a more positive potential, it became almost constant showing limiting nature. This is most likely due to the formation of a salt film, probably of $FeCl_2$ [34] or CuCl or any deposited copper on the surface of the material as the copper content of the steel is 1.48 wt.%. According to the potential–pH–$Cl^-$ diagram of copper [35], copper dissolves as $CuCl_2^-$ or produces CuCl in lower pH solutions containing $Cl^-$ ions. The CuCl thus formed at the metal–electrolyte interface acts as a barrier to the metal ion entering into the solution for which limiting currents were observed at higher potentials. It is also possible that pure metallic copper may get deposited on the surface of the material [36]. The corrosion products precipitated on the alloy surface retarded the dissolution process effectively. SEM studies (Fig. 2b) showed that a powdery corrosion product formed which covered the entire surface though the maximum accumulation was at the grain boundaries. This revealed feeble corrosive intergranular attack. The corrosion products resembled closely to those of copper in NaCl + $H_2SO_4$ aqueous solution [36]. Thus, the deposits were most likely either metallic copper or its chloride salt (CuCl). Usually the copper-containing stainless steels suffer from intergranular corrosion in chloride-containing acidic solutions of methanol [37]. Spectral analysis showed the presence of $Cr^{3+}$ and $Fe^{3+}$ in the electrolytic solution.

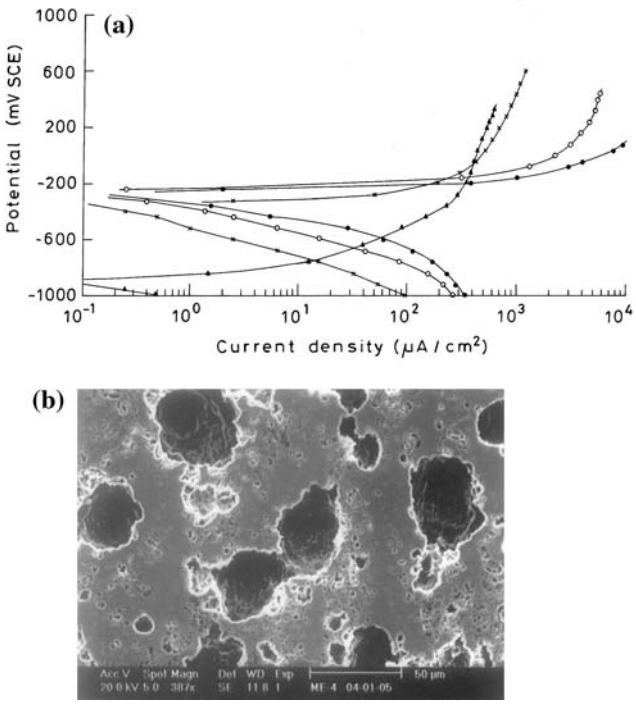


**Fig. 3** (**a**) Polarization curves of nitrogen-containing austenitic stainless steel in different concentrations of LiCl in methanol, at 35°C. (i)▲—▲ 0.001 M LiCl, (ii)×—× 0.01 M LiCl, (iii)o—o 0.1 M LiCl, and (iv) •—• 0.25 M LiCl. (**b**) SEM micrograph of nitrogen-containing austenitic stainless steel after polarization in 0.1 M LiCl in methanol

## Methanol–LiCl

The OCP of the alloy in methanol containing different concentrations of LiCl (0.001–0.25 M) lies between –375 and –100 mV. Figure 3a represents the cathodic and anodic polarization curves of the steel in 0.001–0.25 M LiCl in methanol. The cathodic curves were almost linear and were associated with well-defined Tafel slopes. The current density increased steadily as the concentration of $Cl^-$ ions increased from 0.001 to 0.25 M; however, the currents were much lower than those in the acidic methanol solutions containing the same concentrations of the $Cl^-$ ions. The observed difference can be due to a different cathodic reaction occurring in acid-free chloride solutions than hydrogen evolution in acidic methanol solutions and the expected reaction is the oxygen reduction; the predominant cathodic reaction in neutral methanol.

Like methanol–HCl system, the anodic curves here also showed active dissolution only and the anodic Tafel slopes ($b_a$) ranged from 30 to 75 mV/dec. The corrosion current density ($i_{corr}$) increased in the order 0.001 < 0.01 < 0.1 < 0.25 M. The $i_{corr}$ was 0.074 and 0.35 μA/cm$^2$ for 0.001 and 0.25 M LiCl, respectively. Thus, the observed difference in the corrosion current for the highest and the lowest concentration was not very large, i.e., the rate of corrosion did not differ to a large extent as the concentration of $Cl^-$ ions were increased up to 0.25 M. Further, the $Cl^-$ ion concentration remaining the same (except 1.0 M HCl and 0.25 M LiCl), the $i_{corr}$ for the acidic solution was always higher, although it was less prominent in the lower concentrations, i.e., a small addition of the acid (0.001 and 0.01 M) did not activate the medium effectively to bring out any substantial corrosion. However, when the acid concentration was increased up to 0.1 M, large increase in the corrosion currents was observed (i.e., $i_{corr}$ was 33 μA/cm$^2$ for 0.1 M HCl in comparison to 0.25 μA/cm$^2$ in 0.1 M LiCl). Thus, the rate of corrosion increased by a factor >100 in higher concentrations of HCl solution in compar-

ison with acid-free methanolic chloride solutions. The results clearly indicate the adverse effect of the acid in the most aggressive chloride solutions. Such effect can be due to the promotion of proton reduction in acidic media than the oxygen evolution in neutral methanol solution. In presence of the acid, methanol gets protonated as:

$$CH_3OH + H^+ \rightarrow CH_3OH_2^+ \quad (4)$$

The discharge of $CH_3OH_2^+$ may be associated with lower overvoltage as compared to $H_3O^+$ discharge on cathode [38]. Therefore, it facilitates the cathodic reaction which results in an accelerating effect on the anodic dissolution showing high corrosion rates.

The nature of the anodic polarization curves was quite similar to those in case of methanol–HCl system indicating that at a more positive potential the anodic reaction proceeded under the diffusion control due to precipitation of a salt film on the electrode surface. The corresponding scanning electron micrograph of the exposed specimen in 0.1 M LiCl–methanol (Fig. 3b) revealed apparently shallow pit like structures on the surface which overlapped on each other imparting an irregular shape. However, these are not the real pits as the aggressive chloride ions prevent the formation of any passive film. Rather, the structures are due to the spalling of the loosely bound and less protective corrosion products (salt film) from the surface, formed due to excessive dissolution in the form of $Fe(OH)_3$ which was confirmed by chemical analysis.

## Methanol–HCl + $H_2SO_4$

Figure 4a and 4b illustrates the polarization curves of the steel in solutions containing HCl and $H_2SO_4$ of varying ratio in methanol. The cathodic curves closely resembled in nature to those observed in the case of methanol–$H_2SO_4$ system and the Tafel slopes ($b_c$) ranged between 90 and 140 mV/dec. Therefore, the cathodic reaction can be the activation controlled hydrogen evolution reaction. The current density increased as the acid concentration increased.

The anodic polarization curves present two distinct features. First, the curves showing active anodic dissolution only, and second, with distinct active–passive–transpassive regions. When HCl and $H_2SO_4$ were present in equimolar proportions (0.001 M HCl + 0.001 M $H_2SO_4$, 0.01 M HCl + 0.01 M $H_2SO_4$ and 0.1 M HCl + 0.1 M $H_2SO_4$), no passivation was observed and the steel dissolved actively similar to those observed in the case of methanol–HCl and methanol–$H_2SO_4$ solutions (0.001 M). The corrosion current density ($i_{corr}$) and hence the rate of corrosion increased as the concentration of acids increased from 0.001 to 0.1 M. The corrosion rates in these cases were even larger than those containing $H_2SO_4$ or HCl alone in methanol. It appears that combined activating effect of both the acids enhanced the rate of corrosion significantly.

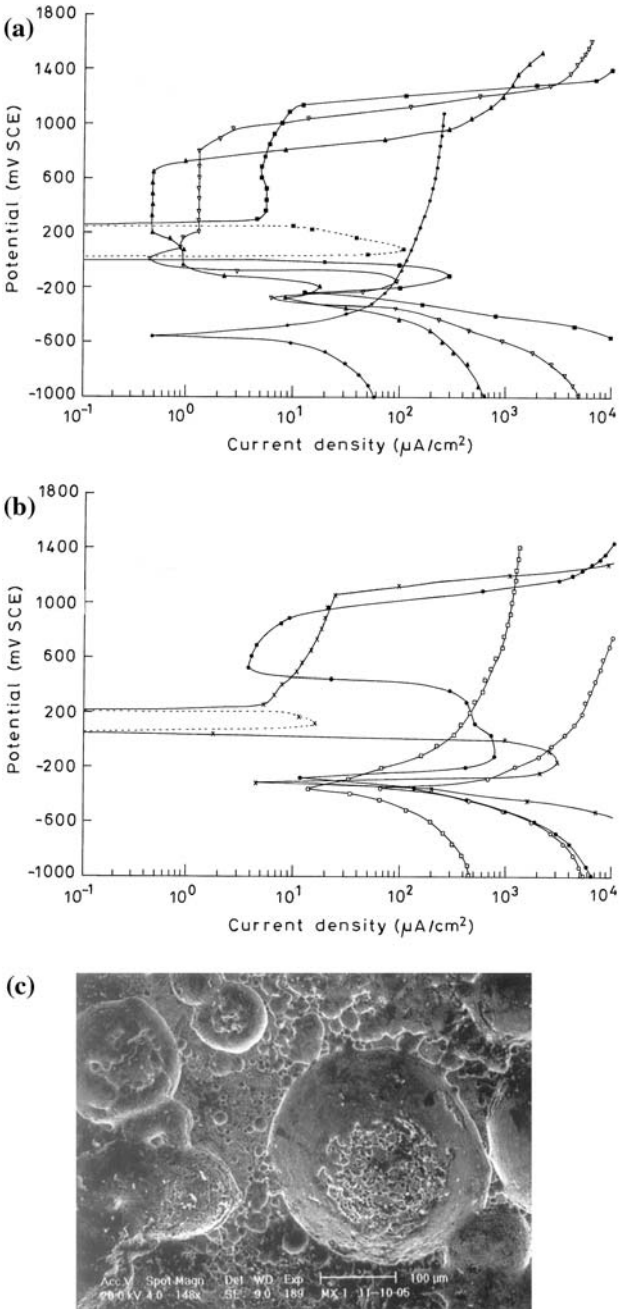


**Fig. 4** (**a**) Polarization curves of nitrogen-containing austenitic stainless steel in methanol–HCl + $H_2SO_4$ solution, at 35°C. (i) ●—● 0.001 M HCl + 0.001 M $H_2SO_4$, (ii)▲—▲ 0.001 M HCl + 0.01 M $H_2SO_4$, (iii) ▽—▽ 0.001 M HCl + 0.1 M $H_2SO_4$, (iv) ■—■ 0.001 M HCl + 1.0 M $H_2SO_4$. (**b**) Polarization curves of nitrogen-containing austenitic stainless steel in methanol–HCl + $H_2SO_4$ solution, at 35 °C. (i) ○—○ 0.1 M HCl + 0.1 M $H_2SO_4$, (ii)□—□ 0.01 M HCl + 0.01 M $H_2SO_4$, (iii)●—● 0.01 M HCl + 0.1 M $H_2SO_4$, and (iv)×—× 0.01 M HCl + 1.0 M $H_2SO_4$. (**c**) SEM micrograph of nitrogen-containing austenitic stainless steel after polarization in 0.01 M HCl + 1.0 M $H_2SO_4$ in methanol

**Table 2** Corrosion parameters of nitrogen-containing austenitic stainless steel in methanol–HCl + $H_2SO_4$ solution, at 35 °C

| Conc. of HCl (M) | Conc. of $H_2SO_4$ (M) | $E_{corr}$ (mV) | $i_{corr}$ (μA/cm$^2$) | $i_{crit.}$ (μA/cm$^2$) | $i_p$ (μA /cm$^2$) | $E_{pass}$ (mV) | $E_{pit}$ (mV) | ($E_{pit}$ ~ $E_{pass}$) (mV) |
|---|---|---|---|---|---|---|---|---|
| 0.001 | 0.001 | –560 | 0.68 | – | – | – | – | – |
| 0.001 | 0.01 | –260 | 7.5 | 18 | 0.48 | –40 | 640 | 680 |
| 0.001 | 0.1 | –280 | 50 | 90 | 1.3 | 0 | 960 | 960 |
| 0.001 | 1.0 | –240 | 45 | 290 | 6.5 | 320 | 1120 | 800 |
| 0.01 | 0.01 | –320 | 10 | – | – | – | – | – |
| 0.01 | 0.1 | –280 | 12 | 750 | 5.7 | 520 | 680 | 160 |
| 0.01 | 1.0 | –280 | 64 | 3000 | 14 | 280 | 1040 | 760 |
| 0.1 | 0.1 | –350 | 94 | – | – | – | – | – |

Active–passive–transpassive behaviour was observed in solutions containing 0.001 M HCl with 0.01–1.0 M $H_2SO_4$ (i.e., for $H_2SO_4$ to HCl concentration ratio 10:1, $10^2$:1 and $10^3$:1) and 0.01 M HCl with 0.1–1.0 M $H_2SO_4$ (i.e., for $H_2SO_4$ to HCl concentration ratio, 10:1 and $10^2$:1). This shows that the passive films are formed only when $H_2SO_4$ to HCl concentration ratio is >~10:1, provided the HCl concentration is below 0.1 M. For a particular HCl concentration, both the $i_{corr}$ and the $i_{crit}$ increased in the order 10:1 < $10^2$:1 < $10^3$:1 indicating increasing rate of the anodic dissolution in the initial active region. Moreover, similar to those in case of 1.0 and 2.0 M $H_2SO_4$ solutions, 'cathodic loop' was also observed in this case in potential regions 40–260 and 80–220 mV for 0.001 M HCl + 1.0 M $H_2SO_4$ and 0.01 M HCl + 1.0 M $H_2SO_4$ solutions, respectively (dashed lines in Fig. 4a and 4b). Thus it is clear that 'cathodic loop' appears only when the concentration of $H_2SO_4$ is >~1.0 M. Similar explanation as given in the case of methanol–$H_2SO_4$ solution seems to be plausible in this case also.

When the $H_2SO_4$ to HCl concentration ratio was increased in the order 10:1 <$10^2$:1 <$10^3$:1, the passivation current density ($i_p$) also increased. At the same time, the passivation potential range ($E_{pit}$ ~ $E_{pass}$) broadened and the breakdown potential shifted in the noble direction (Table 2). The breakdown of the passive film was due to mild pitting attack (Fig. 4c). The passivity in these cases can be considered as due to the inherent water content of the sulphuric acid. However, the shifting of the pitting potential ($E_{pit}$) in the noble direction is probably due to the inhibiting effect of the $SO_4^{2-}$ ions against the aggressive chloride ions responsible for pitting. Earlier studies [39, 40] have shown that the sulphate ions effectively inhibit the chloride induced pitting corrosion. In light of this, it can be extended that the aggressive chloride ions adsorb easily on the passive film which in turn replace the oxygen positions forming soluble metal chlorides and thus pitting is initiated. When sulphate ions are present at sufficiently high concentrations, they get incorporated into the passive film. As a consequence, a coulombic barrier against the chloride adsorption is formed leading to high resistance against pitting. In the transpassive region, limiting currents were observed with evolution of oxygen after potential 1400 mV with few exceptions. The solution after the electrochemical studies developed greenish yellow colour due to the presence of $Fe^{3+}$ and $Cr^{3+}$ ions.

## Conclusions

1. The alloy shows active–passive–transpassive dissolution only at higher concentrations of $H_2SO_4$ (0.01–2.0 M) in methanol, and passivity is due to the existing water content of $H_2SO_4$. However, the passive film becomes unstable as the $H_2SO_4$ concentration increases. The steel exhibits a tendency to suffer from mild pitting attack.
2. In chloride-containing methanolic solutions, the steel exhibits active behaviour only and the rate of corrosion increases significantly as the $Cl^-$ ion concentration is increased. The addition of acid leads to an increase in the corrosion rate by as much as 100 times compared to near neutral chloride solutions. Mild intergranular corrosion occurs in acidic chloride solutions.
3. Even in presence of HCl, passive films are formed when the $H_2SO_4$ to HCl concentration ratio is >~10:1. $SO_4^{2-}$ ions tend to inhibit the pitting attack by increasing the pitting potential.

**Acknowledgement** Financial assistance for this work from Council of Scientific and Industrial Research (CSIR), New Delhi, India is gratefully acknowledged.

## References

1. Vanini AS, Audouard JP, Marcus P (1994) Corros Sci 36:1825
2. Flis J, Kuczynska M (2004) J Electrochem Soc 151:B573
3. Leckie HP, Uhlig HH (1966) J Electrochem Soc 113:1262

4. Hermas AA, Ogura K, Takagi S, Adachi T (1995) Corrosion 51:3
5. Bandy R, Van Rooyen D (1983) Corrosion 39:227
6. Bayoumi FM, Ghanem WA (2005) Mater Lett 59:3311
7. Mudali UK, Reynders B, Stratmann M (1999) Corros Sci 41:179
8. Tsai WT, Reynders B, Stratmann M, Grabke HJ (1993) Corros Sci 34:1647
9. Clayton CR, Halada P, Kearns R (1995) Mater Sci Eng A 198:135
10. Pawlick LA, Kelly RG (1995) J Corros Sci Eng 1:15
11. Singh VB, Upadhyay BN (1998) Corros Sci 40:705
12. Singh VK, Singh VB (1988) Corros Sci 28:385
13. Singh VB, Gupta A (2005) Ind J Chem Tech 12:347
14. Keller P, Strehblow HH (2004) Corros Sci 46:1939
15. Wilde BE, Hodge FG (1969) Electrochim Acta 14:619
16. Rozenfeld IL (1981) Corrosion 37:371
17. Greene ND (1960) J Electrochem Soc 107:4571
18. Lee JW, Osseo-Asare K, Pickering HW (1985) J Electrochem Soc 132:550
19. Frankenthal RP (1967) J Electrochem Soc 114:542
20. Hermas AA, Ogura K, Adachi T (1995) Electrochim Acta 40:837
21. Mazza F, Torchio S, Ghislandi N (1984) In: Proceedings of the 9th international congress on metallic corrosion, Toronto, vol. I, p 102
22. Szklarska -Smialowska Z, Mankowski J (1982) Corros Sci 22:1105
23. Umebayashi R, Akao N, Hara N, Sugimoto K (2003) J Electrochem Soc 150:B295
24. Zhang YS, Zhu XM (1999) Corros Sci 41:1817
25. Yang WP, Costa D, Marcus P (1994) J Electrochem Soc 141:2669
26. Asami K, Hashimoto K, Musumoto T, Shimodaira S (1976) Corros Sci 16:909
27. Clayton CR, Olefjord I (2002) In: Corrosion mechanism in theory and practice. Marcel Dekker, New York, p 217
28. Mansfeld F (1973) J Electrochem Soc 120:188
29. El-Naggar MM (2006) Applied Surf Sci R52:6179
30. Szklarska-Smialowska Z (1984) In: Proceedings of the 9th international congress on metallic corrosion, Toronto, vol. II, p 112
31. Tromans D, Ahmed T (1998) J Electrochem Soc 145:601
32. Cerquetti A, Mazza F (1973) Corros Sci 13:337
33. Badawy WA, Ismail KM, Fathi M (2005) Electrochim Acta 50:3603
34. Pistorius PC, Burstein GT (1992) Corros Sci 33:1885
35. Van Muylder J, Dezoubov N, Pourbaix M (1962) Report 101, CEBELCOR, Brussels, Belgium
36. Ujiro T, Satoh S, Staehle RW, Smyrl WH (2001) Corros Sci 43:2185
37. Ogura S, Sugimoto K, Sawada Y (1976) Corros Sci 16:323
38. Singh DDN, Gaur B, Ghosh R, Singh BK (1998) NML Tech J 40:77
39. Carranza RM, Alvarez MG (1996) Corros Sci 38:909
40. Barbucci A, Cerisola G, Cabot PL (2002) J Electrochem Soc 149:B534